NASA TECHNICAL MEMORANDUM

N73. 26841

NASA TM X- 62,279

NASA TM X- 62,279

IRON ABUNDANCE IN THE MOON FROM MAGNETOMETER MEASUREMENTS

Curtis W. Parkin, Palmer Dyal, and William D. Daily

University of Santa-Clara
Santa Clara, Calif. 94053
and
Ames Research Center
Moffett Field, Calif. 94035

April 1973

Iron abundance in the moon from magnetometer measurements

CURTIS W. PARKIN

Department of Physics, University of Santa Clara,
Santa Clara, California 94053

PALMER DYAL and WILLIAM D. DAILY
NASA-Ames Research Center
Moffett Field, California 94035

Abstract--Apollo 12 and 15 lunar surface magnetometer data with simultaneous lunar orbiting Explorer 35 data are used to plot hysteresis curves for the whole moon. From these curves a whole-moon permeability $\mu = 1.029 \, ^{+0.024}_{-0.019}$ is calculated. This result implies that the moon is not composed entirely of paramagnetic material, but that ferromagnetic material such as free iron exists in sufficient amounts to dominate the bulk lunar susceptibility. From the magnetic data the ferromagnetic free iron abundance is calculated. Then for assumed compositional models of the moon the additional paramagnetic iron is determined, yielding total lunar iron content. The calculated abundances are as follows: ferromagnetic free iron, 5 ± 4 wt. %; total iron in the moon, 9 ± 4 wt %.

INTRODUCTION

In this paper we calculate lunar iron abundance from simultaneous magnetic field measurements made by instruments on the lunar surface and in orbit near the moon. The total iron abundance is the sum of metallic free iron and chemically combined iron, calculated for suitable compositional models of the lunar interior.

Previous estimates of whole-moon iron abundance have generally been ~ 10% by weight, often based on meteoritic compositional models, using the lunar density of 3.34 g/cm^3 as a constraint. Urey (1962) reported that the moon, if composed of chondritic material of proper density, would have 11-14% iron by weight, depending upon the high pressure phases present in the moon. Reynolds and Summers (1969), using a mathematical model involving equations of state at high pressure, placed a value of 13% on lunar iron abundance. Later Urey and MacDonald (1971) estimated values of 5% total iron using a model in which all the iron is present as FeO, and 8.65% total iron for another model in which the iron is combined in equal amounts of FeO and FeS. Wänke et al.(1973) reported a value of 9%, modeling lunar composition by that of the Allende chondritic meteorite. These previous results are generally consistent with the whole-moon iron abundance calculated in this paper.

We calculate lunar iron content from whole-moon magnetic hysteresis curves. These curves are plots of total surface magnetic field measured by Apollo 12 and 15 surface magnetometers simultaneous with the external field measured by the lunar orbiting Explorer 35 magnetometer. The slopes of the hysteresis curves are used to calculate magnetic permeability of the moon, from which we can calculate total iron content in the lunar interior. A paramagnetic mineral (olivine or orthopyroxene), combined with ferromagnetic free iron, is used with the lunar density constraint to calculate the iron abundance.

THEORY

A lunar hysteresis curve is plotted using data obtained during times when the lunar sphere is magnetized by the earth's magnetic field. The total magnetic field $\underline{B}$ measured at a magnetometer site on the lunar surface is, in electromagnetic units,

$$\underline{B} = \underline{H} + 4\pi\underline{M} , \tag{1}$$

where $\underline{H}$ is the steady external (terrestrial) magnetizing field and $\underline{M}$ is the magnetization field induced in permeable lunar material. (see Fig.1) Alternately, equation (1) can be expressed $\underline{B} = \mu \underline{H}$, where the relative permeability $\mu = 1 + 4\pi k$; k is magnetic susceptibility in emu/cm^3.

The lunar interior is modeled by a homogeneous sphere which has an iron Curie point (T_c) isotherm at some depth R/R_{moon}. The sphere is assumed to be composed/ of a paramagnetic mineral with free iron distributed throughout. The free iron is ferromagnetic in the outer shell where $T < T_c$, and paramagnetic in the core where $T > T_c$. The permeability μ_2 of the core therefore corresponds to paramagnetic material only, while μ_1 of the shell combines contributions from ferromagnetic iron and a paramagnetic mineral.

Following the method of Jackson (1962) the total field on the outer surface of the sphere can be expressed in vector component form (see APPENDIX for details):

$$\underline{B} = H_x(1+2F)\hat{x} + H_y(1-F)\hat{y} + H_z(1-F)\hat{z} \tag{2}$$

where

$$F = \frac{(2\eta+1)(\mu_1-1) - \lambda^3(\eta-1)(2\mu_1+1)}{(2\eta+1)(\mu_1+2) - 2\lambda^3(\eta-1)(\mu_1-1)} \tag{3}$$

Here $\eta = \mu_1/\mu_2$; μ_1 and μ_2 are relative permeability of shell and core respectively (permeability of free space $\mu_0 = 1$); $\lambda = R_2/R_1$, where R_2 = radius of the core and R_1 = radius of the whole sphere. The components of $\underline{B}$ are expressed in the ALSEP coordinate system which has its origin on the lunar surface at a magnetometer site. The x-axis is directed radially outward from the lunar surface; the y and z axes are tangential to the surface, directed eastward and northward, respectively.

Once field measurements of $\underline{H}$ and $\underline{B}$ have been used to determine a value for F, iron abundances can be calculated for suitable lunar compositional models which must meet the additional constraints imposed on the lunar sphere by the overall lunar bulk density (3.34 g/cm^3) and moment of inertia. The core radius R_2 is determined by the iron Curie temperature where, because of internal temperature and pressure (Bozorth, 1951), iron changes from the ferromagnetic to the paramagnetic state. It is assumed that the core material has only paramagnetic susceptibility k_2 ($\mu_2 = 1 + 4\pi k_2$) and that the temperature variation of the paramagnetic susceptibility varies according to the Langevin theory:

$$k = n\, m^2/3K\, T , \qquad (4)$$

where K is the Boltzmann constant, T is absolute temperature, n is the number of ions per gram, and m is the atomic moment. m is of the order of a few Bohr magnetons μ_B; e.g., for the Fe^{2+} ion, m = 5.25 μ_B to 5.53 μ_B (Nagata, 1961).

In the outer shell where temperature $T < T_c$, the susceptibility $k_1 = k_{al} +$ "apparent" k_{pl}, where k_{al} is ferromagnetic susceptibility and k_{pl} is paramagnetic susceptibility. The ferromagnetic component is metallic free iron, assumed to be composed of multidomain, noninteracting grains. Furthermore, the expected pressures and temperatures in the outer shell are such that the ferromagnetic susceptibility of iron will not be substantially altered (Bozorth, 1951; Kapitsa, 1955).

The measured ferromagnetic susceptibility of the shell material is an apparent value which differs from the intrinsic ferromagnetic susceptibility of the iron because of self-demagnetization of the iron grains and the volume fraction of iron in the shell. The apparent ferromagnetic susceptibility k_{al} is related to the intrinsic susceptibility k_{fl} according to

$$k_{al} = \frac{p \, k_{fl}}{1 + N \, k_{fl}} \, , \tag{5}$$

where N is the demagnetization factor and p is the volume fraction of the iron. For spherical iron grains $N = 4 \, \pi/3$; experimentally N is found to range between 3 and 4 (Nagata, 1961). We shall use $N = 3.5$ in our calculations.

EXPERIMENTAL TECHNIQUE

The basic technique uses simultaneous magnetometer measurements of the fields $\underline{B}$ and $\underline{H}$, made while the moon is in the quiet geomagnetic tail region (see Fig. 2). The total surface field $\underline{B}$ is measured by lunar surface magnetometers (LSM) at the Apollo 12, 15, and 16 sites. The LSM instrument properties are described in detail by Dyal et al. (1972). Simultaneous measurements of the geomagnetic tail field $\underline{H}$ are made by the lunar orbiting Explorer 35 magnetometer, which orbits the moon with 0.5 R_{moon} periselene and 5 R_{moon} aposelene at a period of 11.5 hours. The Explorer 35 orbit is displayed in a companion paper in this volume (Dyal et al., 1973), and detailed instrument characteristics are outlined by Sonett et al., (1967).

/Fig. 2

1. Lunar induction in the geomagnetic field

The geomagnetic tail consists of two regions ("lobes") of differing magnetic polarity, associated with the earth's dipole field extended downstream in the solar wind. At about 60 earth radii the lunar orbit intersects the magnetic tail as indicated by the accented portion of the orbit shown in Fig. 2, and the moon is in the geomagnetic tail field about four days of each lunation. The magnetic and plasma morphology of the geotail are especially favorable for observing the steady state induced magnetization field of the moon. The ambient field in the geotail is steadier and more uniform than in any other magnetic region of the lunar orbit. The geomagnetic field shields the moon from the solar plasma, minimizing electromagnetic interaction effects other than the magnetization field.

In general the total magnetic field at the lunar surface is a vector sum of the external magnetic field measured by Explorer 35; the steady remanent field at the LSM site; the poloidal field resulting from transverse electric (TE) induction; the toroidal field resulting from transverse

magnetic (TM) induction; the magnetization field induced in the permeable

material within the moon; the diamagnetic field associated with the plasma-

moon interface currents; and the field associated with the dynamical inter-

action between plasma flow and the lunar fields. A careful consideration

of each of these contributions to the total field at the lunar surface is

necessary to justify the data selection and analysis best suited to determine

accurately the magnetization fields of the moon in the geomagnetic environment.

We will see that some of these fields are important to our analysis while

contributions from others can be neglected.

The solution given by equations (2) and (3) for the magnetization of the

moon assumes a uniform external magnetizing field. Under this assumption

the induced field is dipolar; higher order multipoles contribute when

inhomogeneities are present in the external field. Uniformity of the ambient

geotail field cannot be guaranteed with the available data. It is possible

to discriminate against data from nonuniform tail fields by requiring magnetic

conditions at both LSM and explorer instruments simultaneously to be steady

over long time intervals. If the geomagnetic field and moon are in relative

motion with a speed characterized by $V \gtrsim L/T$, where L is the distance between

LSM and Explorer 35 magnetometers and T is the time over which the field is

steady, then any nonuniformities can be detected as magnetic fluctuations at

either instrument. Various criteria on the peak-to-peak fluctuations at both

magnetometers have been used to select data. A summary of the data selection

criteria will be presented in a later subsection.

Fluctuations of the geotail field $(\frac{\partial B_E}{\partial t})$ drive time-dependent eddy currents in the

lunar interior. These in turn result in/poloidal magnetic field (TE induction)

which is probably the largest of the electromagnetic induction fields measured

at the surface. In the limit of low-frequency or small-amplitude driving field

$\partial B_E/\partial t \to 0$ and

fluctuations,/induction from the /mode vanishes. Therefore the restrictions
poloidal

-7-

placed on the peak-to-peak variations of surface and external fields, used to discriminate against nonuniform geotail fields, will simultaneously eliminate data obviously contaminated by eddy current fields. Furthermore, the data averaging procedures used in the analysis tend to filter out the higher frequencies which are the major contributors in this mode.

Relative motion of the moon and the geomagnetic field results in a motional electric field $\underline{E}_m = \underline{V} \times \underline{H}$ in the lunar reference frame, where $\underline{V}$ is the relative lunar velocity and $\underline{H}$ is the external field. Currents driven by $\underline{E}_m$ set up magnetic fields (TM induction) that are toroidal about the electric field. Theoretically this magnetic field is everywhere tangent to the lunar surface so that the ALSEP x-components contain minimal toroidal induced fields.

If the induced magnetization field $\underline{B}_o \propto \frac{4\pi M}{}$ is predominately dipolar, the dipole axis will be aligned with the external field, $\underline{H}$. At the lunar surface the radial and tangential components of the dipole field are (see Appendix) $B_{or} = 2\alpha\cos\theta$ and $B_{o\theta} = \alpha\sin\theta$, where θ is the angle between the dipole axis and the radius vector to the surface site, and α is the dipole moment. We see that the maximum radial component is along the dipole axis, which for the average geomagnetic tail field is along the earth-sun line. As a result the average surface dipole field at both Apollo 12 and Apollo 15 LSM sites is predominantly in the radial or ALSEP $\hat{x}$ direction.

As plasma particles spiral about magnetic field lines, their motion induces an opposing field resulting in plasma diamagnetism. The solar wind plasma diamagnetism has been detected by Colburn et al. (1967) and is seen as a magnetic field increase $(\underline{B}_d)$ of about 1.5 gammas in magnitude in the plasma void on the antisolar side of the moon. This diamagnetic field can be expressed (Boyd and Sanderson, 1969):

$$B_d \propto N_i(T_e + T_i)/H \quad .$$

H is ~~magnitude of~~ the external vacuum field, N_i is the plasma ion density, and T_e and T_i are the electron and ion temperatures perpendicular to the magnetic field $\underline{H}$. The average tail magnetic field is about 10 gammas while the plasma density is at least two orders of magnitude below average solar wind values. Little is known of the tail plasma temperature, but it is probably $\lesssim 10^5$ °K. An upper limit on B_d in the geotail is therefore ~ 0.03 gamma, which is far below the LSM resolution of 0.2 gamma. Therefore plasma dia-magnetism will be neglected in this analysis.

The dynamic interaction between solar wind plasma and the lunar surface fields have been found to be $\leq 16\gamma$ and $\leq 1\gamma$ at Apollo 12 and 15 sites respectively (Dyal et. al., 1973). Plasma streaming pressure responsible for compression of surface fields is $(1/2)N_i mv^2$ where m is the proton mass and v is the plasma bulk speed. We assume a typical speed in the tail is characterized by the average magnetopause motions which are about 70 km/sec (Mihalov et al., 1970). Inside the magnetotail lobes the plasma density is below about $0.01/cm^3$. Therefore the plasma-field interaction in the geotail has to be at least 10^3 times weaker than in the free streaming solar wind and can be neglected.

Since remanent surface field compression is negligible, it will be assumed that the steady remanent fields at both LSM sites are constant in the tail, the importance of which will soon be apparent. In addition these fields are assumed to be not measurable by Explorer 35 at periselene. The results of the Apollo subsatellite magnetometer reported by Sharp et al. (1972) confirm this assumption. Therefore Explorer 35 measures only the external geomagnetic field.

2. Data processing criteria

Magnetization effects can be maximized and competing electromagnetic induction minimized by applying data selection criteria. It has been pointed out that at the Apollo 12 and 15 sites the magnetization field is largest in

the radial or ALSEP x-axis. Furthermore, toroidal mode fields are not
present in the x-component and plasma interaction effects are minimal along
the x direction. Therefore, only the ALSEP x-components of the LSM and
Explorer 35 data have been used to calculate magnetization fields. Several
averaging intervals (6 minutes, 15 minutes, 30 minutes, 1 hour) were used for
analysis of Apollo 12 data, each with different peak-to-peak criteria, to
insure external field uniformity and minimize poloidal field contamination.
Only 60-minute and 3-hour averages, without peak-to-peak criteria, were
useful for the Apollo 15 data since the simultaneous Explorer 35 data were
contaminated by a high-frequency satellite spin-modulated tone. A typical
30-minute swath of Apollo 12 data used in the analysis is shown in Fig. 3. 〈Fig. 3
The steadiness of these data is characteristic of much of the geomagnetic
tail field.

3. Lunar Hysteresis curves

Typical lunar "hysteresis" curves are shown in Fig. 4. Apollo 12 and   〈Fig. 4
15 averages of x components are plotted on the abscissa with the simultaneous
Explorer 35 averages on the ordinate. These data were taken from four luna-
tions of Apollo 12 and two lunations of Apollo 15 data. Bifurcation in the
distributions is a result of the data selection criteria which eliminate
data from near the neutral sheet. The normal "S" shape of the hysteresis
curve degenerates at these low field values to a straight line (Ellwood, 1934)
intersecting the origin since the x axis intercept (x-component of the remanent
field at both sites) has been subtracted from the data.

4. Statistical Analysis

Four lunations of Apollo 12 data and two of Apollo 15 data have been
processed for each of the averaging times, employing the data selection criteria
described previously. This has resulted in a total of six separate hysteresis
curves, one for each averaging interval of both instruments. To each of these

data sets a least squares straight line has been fitted. The average and standard deviation values of the slopes are 1.019 ± 0.012. Both extrema are greater than 1.0, implying that the moon, as a whole, acts as a para-magnetic or weakly ferromagnetic sphere.

Scatter in the Apollo 12-Explorer 35 data points of Fig. 4(a) is primarily a result of magnetic inhomogeneities between the moon and Explorer 35, small contributions from eddy current fields, and instrumental noise in the Apollo and Explorer magnetometers. These error sources may introduce small random fluctuations into the data which will not substantially affect the slope or intercept of the least-squares line. An error source which could affect the least-squares slope is a time-dependent heading drift of the Explorer 35 magne-tometer. The drift problem, which began after the Apollo 12 and Explorer 35 data used in Fig. 4(a) were acquired, is therefore applicable only to analysis of simultaneous Explorer 35 and Apollo 15 data. The slope of the Apollo 15-Explorer 35 hysteresis curve (1.019 ± 0.004) shown in Fig. 4(b) agrees well with that obtained from the Apollo 12-Explorer 35 curve (1.019 ± 0.013), however, indicating that the Explorer 35 heading error is minimal for the time periods used in Fig. 4(b). Furthermore, the agreement in the analysis of data from these two Apollo surface sites, which are separated by 1000 km, is a good test of our assumption of lunar azimuthal symmetry.

RESULTS

1. Bulk magnetization properties of the lunar sphere

It is shown in the Theory section that the slope of the hysteresis curve
at very low field values is related to the magnetic susceptibility of the
moon. Fig. 5 relates F of equation (3) to the susceptibilities k_1 and k_2
of the lunar shell and core. The curve $\epsilon = k_1/k_2 = 1$ corresponds to the case
of a magnetically homogeneous sphere of permeability $\mu = 1 + 4\pi k_1$,
from which bulk permeability of the moon is calculated to be $\mu = 1.029\,^{+0.024}_{-0.019}$.
Error limits are one standard deviation.
Since both upper and lower limits of permeability are above 1.0, the moon as
a whole responds magnetically as a paramagnetic or weakly ferromagnetic sphere.
The field at the surface is in general a function of both shell and core sus-
ceptibilities; as the susceptibility ratio $\epsilon = k_1/k_2$ increases, the core
susceptibility k_2 becomes less important magnetically, and the family of
curves merge for $\epsilon \gtrsim 100$.

A further use of the bulk lunar permeability is to place limits on the
magnetic dipole moment induced in the moon by the geomagnetic field. The dipole
moment is $HR_1^3 F$ (see Appendix); it is oriented parallel to the external field,
and for $H = 10$ gammas, the induced dipole moment is of magnitude $5.0 \pm 3.2 \times 10^{23}$
gammas-cm^3. Russell et al. (1973) using subsatellite magnetic data, have placed
an upper limit on the permanent lunar dipole of 1.7×10^{23} gammas-cm^3. While
interesting to compare, these two results are for different phenomena. The
averaging techniques performed over many subsatellite orbits to obtain the
permanent dipole value may effectively average out the magnetization fields
which change magnitude and polarity as a function of the external field $\underline{H}$.

2. Lunar composition and iron abundance

In this section we calculate iron abundance in the moon, using various compositional models of the lunar interior. The models are constrained by magnetic permeability, temperature, pressure, density, and moment of inertia determinations.

The lunar moment of inertia is approximately that of a sphere of homogeneous density (Ringwood and Essene, 1970). We will constrain our lunar models to be of uniform density $\rho = 3.34$ gm/cm^3 throughout.

We have selected two paramagnetic minerals to model the lunar interior: olivine and orthopyroxene. In the moon's outer shell, free iron is assumed to be interspersed throughout the paramagnetic rock matrix. These minerals, with iron content constrained by the overall density of 3.34, have properties which are consistent with measured seismic velocity profiles at mantle depths (Toksöz et al., 1972) and geochemical considerations (Ringwood and Essene, 1970; Green et al., 1971; Gast, 1972). Furthermore, pyroxenes and olivines have been reported to be major mineral components of lunar surface fines and rock samples (Nagata et al., 1971; Zussman, 1972; Weeks, 1972), with combined iron present as Fe^{2+}. The ferromagnetic component of lunar samples is primarily metallic iron (Nagata et al., 1972; Pearce et al., 1971) most of which is thought to be native to the moon rather than meteoritic in origin (Strangway et al., 1973).

Magnetization of the lunar sphere, as measured by the Apollo-Explorer 35 magnetometer network, imposes a magnetic constraint on the lunar composition. This constraint is determined by the hysteresis-curve slope, represented by the value $F = 0.0095 \pm 0.0060$ (see equations (2) and (3)); F is in turn related to the internal susceptibility of the moon.

The Curie point of metallic iron will defines the boundary between a homogeneous shell of susceptibility k_1 and a homogeneous core of susceptibility k_2. The boundary is located using the temperature profiles proposed for the

Fig. 6

moon by several authors as shown in Fig. 6. Also plotted is the Curie temperature of iron which is a function of pressure and therefore of depth (Bozorth, 1951).

For the calculations that follow, three temperature models are used in an effort to match "hot," "warm," and "cold" models. For the hot model the Curie point is at $\lambda = R_2/R_1 = 0.9$. We assume shell and core temperatures are 600 $^{\circ}$C and 1400 $^{\circ}$C, respectively. For the warm model the shell temperature is 500 $^{\circ}$C and that of the core is 1300 $^{\circ}$C, while the boundary is at $\lambda = 0.85$. Temperatures are 300 $^{\circ}$C and 700 $^{\circ}$C for shell and core of the cold model, which has $\lambda = 0.7$. The magnetic properties of the core are entirely determined by the paramagnetism of olivine (Nagata et al., 1957) and orthopyroxene (Akimoto et al., 1958) and the Langevin temperature dependence of these minerals (see equation (4)). Small amounts of free iron will not substantially change the total effective suscepti- bility of the core since iron is paramagnetic above its Curie temperature.

Crustal susceptibility will be determined by the free and combined iron under the assumption that the free iron is in noninteractive, multi- domain grains whose shape demagnetizing factor is on the average 3.5 (Nagata, 1961). Normally the ferromagnetism of free iron is dominated by a dependence on pressure and temperature. However at very low field strengths, such as those of the geomagnetic tail, the susceptibility of iron is not strongly dependent on temperature below the Curie point (Bozorth, 1951). Uniaxial stress on iron changes its susceptibility (Kern, 1961); however, hydrostatic stress should not affect the susceptibility (Kapitsa, 1955) unless, at great pressures, there is a change in volume (Breiner, 1967). Therefore, it will be assumed that the susceptibility of free iron in the shell is independent of pressure and temperature.

Using the constraints outlined above, forward calculations have been made to determine the iron content in the moon. Olivine (10 mole % Fe_2SiO_4) and orthopyroxene (25 mole % $FeSiO_3$) minerals are selected using the bulk lunar density constraint. For a given temperature model Langevin's law yields a range of susceptibilities for each core composition (see Fig. 7) from which the paramagnetic iron content of the core is calculated.

Core susceptibility is then used, along with the magnetically determined range of F, to define a range of susceptibility for the shell. Apparent susceptibility of the shell is then a function of the free and combined iron in the shell. In all cases it is found that the shell susceptibility cannot be accounted for by the paramagnetic susceptibility (k_{pl}) alone; rather, the apparent ferromagnetic susceptibility (k_{al}) is dominant: $k_{al}/k_{pl} \sim 100$. Therefore, using equation (5) the shell free iron abundance is determined to account for the range of F values (see Fig. 5). Finally, the paramagnetic rock matrix of the shell is chosen so that, containing the free iron, it matches the bulk lunar density. Both the ferromagnetic and paramagnetic iron content of the shell are then determined.

From these calculations it has been found that the paramagnetism of any olivine and orthopyroxene cannot account for the measured bulk permeability of the moon; contributions from free iron or other highly permeable material are necessary. When metallic iron is included in a relatively thin outer shell ("hot" model where $\lambda \geq 0.9$), it is difficult to account for the measured bulk permeability of the moon while still maintaining the constraint of homogeneous density throughout the moon.

When the iron Curie point is assumed to be deeper in the moon, i.e., $\lambda=0.85$ ("warm" model) or $\lambda=0.7$ ("cold" model), magnetic permeability and density constraints can be easily satisfied by our compositional models. Ferromagnetic iron content in the shell is the same for both olivine and orthopyroxene,

but is a function of thermal model. The warm model requires 2 to 9 wt.% free iron in the shell, whereas the cold model requires 1 to 5 wt.%. The total iron abundance, on the other hand, is the same for both thermal models, but different for the two mineral compositional models. For olivine (mole % $Fe_2SiO_4 \leq 10\%$) total iron is 5 to 6 wt.%; for orthopyroxene (mole % $FeSiO_3 \leq 25\%$), total iron is 12 to 13 wt.%. The iron abundance limits reported here all include the one-standard-deviation limits of the measured hysteresis curve slope $1.019^{+}_{-}0.012$. Results are summarized in Fig. 8.

Fig. 8

SUMMARY AND CONCLUSIONS

1. Apollo 12 and 15 lunar surface magnetometer data, simultaneous with Explorer 35 magnetometer data, are used to plot hysteresis curves for the whole moon; from these curves a whole-moon permeability $\mu=1.029^{+0.024}_{-0.019}$ is calculated. Both error limits constrain the permeability to be greater than 1.0, implying that the moon as a whole is paramagnetic or weakly ferromagnetic.

2. The permeability calculation places a constraint on the composition of the lunar interior. When the moon is modeled by homogeneous paramagnetic material (olivine or orthopyroxene) of density 3.34 gm/cm^3, it is found that these purely paramagnetic models have magnetic permeabilities far lower than the range determined from magnetometer measurements. We have found no reasonable paramagnetic mineral or combination of minerals, with the correct lunar density, that would have permeability high enough to be consistent with our measured values. From this we infer that the moon must contain some material in the ferromagnetic state, such as free metallic iron, in order to account for the measured global permeability.

3. The paramagnetic-ferromagnetic combination is investigated using a two-layer lunar model; the boundary between the layers is determined by the location of the iron Curie point. Three thermal models, "hot", "warm", and "cold", are used to establish the Curie isotherm location. "Warm" and "cold" models fit both the density and permeability constraints whereas the "hot" models do not. We conclude that the ferromagnetic free iron abundance of the outer shell is 2 to 9 wt.% for "warm" and 1 to 5 wt.% for "cold" models, yielding an overall range of 5±4 wt.%. The free iron content is dependent upon the volume of lunar material below the Curie temperature and independent of the composition of the nonferromagnetic portion of the moon.

4. For two compositional models the total iron abundance is calculated (see Fig. 8). Including both the olivine and orthopyroxene models, the total iron is independent of the thermal model used and is within the limits of 9±4 wt.%.

-17-

REFERENCES

Akimoto S., Hôrai K., and Boku T. (1958) Magnetic susceptibility of orthopyroxene. J. Geomag. Geoelect. 10, 7-11.

Behannon K.W. (1968) Intrinsic magnetic properties of the lunar body. J. Geophys. Res. 73, 7257-7268.

Boyd T.J. and Sanderson, J.J. (1967) Plasma Dynamics. Barnes and Noble.

Bozorth R.M. (1951) Ferromagnetism. D. Van Nostrand.

Breiner S. (1967) The Piezomagnetic effect on seismically active areas, Final Report No. E 22-76-67(N), Dept. of Geophysics, Stanford University.

Colburn D.S., Currie R.G., Mihalov J.D., and Sonett C.P. (1967) Diamagnetic solar-wind cavity discovered behind the moon, Science 168, 1040-1042.

Dyal P. and Parkin C.W. (1972) Lunar properties from transient and steady magnetic field measurements. The Moon 4, 63-87.

Dyal P., Parkin C.W., and Cassen P. (1972) Surface magnetometer experiments: Internal lunar properties and lunar surface interactions with the solar plasma. "Proc. Third Lunar Sci. Conf., Geochim. Cosmochim. Acta" Suppl. 3, vol. 3, pp. 2287-2307. MIT Press.

Dyal P., Parkin C.W., and Daily W.D. (1973) Surface magnetometer experiments: Internal lunar properties, submitted to "Proc. Fourth Lunar Sci. Conf., Geochim. Cosmochim. Acta" Suppl. 3, Vol. 3.

Ellwood W.B. (1934) A new ballistic galvanometer operating in high vacumn. Rev. Sci. Inst. 5, 300-305.

Fricker P.E., Reynolds R.T., and Summers A.L. (1967) On the thermal history of the moon. J. Geophys. Res. 72, 2649-2663.

Gast P.W. (1972) The chemical composition and structure of the moon. In Lunar Geophysics (editors Z. Kopal and D. Strangway), pp. 630-657, Lunar Science Institute Contribution No. 86, Houston. D. Reidel.

Green D.H., Ringwood A.E., Ware N.G., Hibberson W.O., Major A., and Kiss E.
(1971) Experimental petrology and petrogenesis of Apollo 12 basalts.
"Proc. Second Lunar Sci. Conf. Geochim. Cosmochim. Acta" Suppl. 2, Vol. 1,
pp. 601-615. MIT Press.

Hanks T.C. and Anderson D.L. (1972) Origin, evolution and present thermal
state of the moon. Phys. Earth Planet. Interiors 5, 409-425.

Jackson J.D. (1962) Classical Electrodynamics. John Wiley and Sons.

Kapitsa S.P. (1955) Magnetic properties of igneous rock under mechanical
stresses, Bull. (I.V.) Acad. Sci. USSR, Geophys. Ser. No. 6.

Kern J.W. (1961) The effect of stress on the susceptibility and magneti-
zation of a partially magnetized multidomain system. J. Geophys. Res.
66, 3807-3816.

McConnell R.K. Jr., McClaine L.A., Lee D.W., Aronson J.R., and Allen R.V.
(1967) A model for planetary igneous differentiation, Rev. Geophys. 5,
121-172.

Mihalov J.D., Colburn D.S., and Sonett C.P. (1970) Observations of magneto-
pause geometry and waves at the lunar distance. Planet. Space Sci. 18,
239-258.

Nagata T. (1961) Rock Magnetism. Markzen Co. Ltd.

Nagata T., Yukutake T., and Uyeda S. (1957) On magnetic susceptibility of
Olivines. J. Geomag. Geoelect. 9, 51-56.

Nagata T., Fisher R.M., Schwerer F.C., Fuller M.D., and Dunn J.R. (1971)
Magnetic properties and remanent magnitization of Apollo 12 lunar
materials and Apollo 11 lunar microbreccia. "Proc. Second Lunar Sci.
Conf., Geochim. Cosmochim. Acta" Suppl. 2, Vol. 3, pp. 2461-2476.
M.I.T. Press.

Nagata T., Fisher R.M., Schwerer F.C., Fuller M.D., and Dunn J.R. (1972)
Rock magnetism of Apollo 14 and 15 materials. "Proc. Third Lunar
Sci. Conf. Geochim. Cosmochim. Acta" Suppl. 3, Vol. 3, pp. 2423-2447.
MIT Press.

Pearce G.W., Strangway D.W., and Larson E.E. (1971) Magnetism of two
Apollo 12 igneous rocks, "Proc. Second Lunar Sci. Conf. Geochim.
Cosmochim. Acta" Suppl. 2, Vol. 3, pp. 2451-2460. MIT Press.

Pearce G.W., Strangway D.W., and Gose W.A. (1972) Remanent magnetization
of the lunar surface. "Proc. Third Lunar Sci. Conf. Geochim. Cosmochim.
Acta" Suppl. 3, Vol. 3, pp. 2449-2464. MIT Press.

Reynolds R.T. and Summers A.L. (1969) Calculations on the composition of the
terrestrial planets. J. Geophys. Res., 74, 2494-2511.

Ringwood A.E. and Essene E. (1970) Petrogenesis of lunar basalts and the
internal constitution and origin of the moon. Science 167, 607-610.

Russell C.T., Coleman P.J., Lichtenstein B.R., Schubert G., and Sharp L.R.
(1973) Apollo 15 and 16 subsatellite measurements of the lunar magnetic
field (abstract). "In Lunar Science - IV" (editors J.W. Chamberlain
and C. Watkins) pp. 645-646, Lunar Science Institute, Houston.

Sharp L.R., Coleman P.J., Lichtenstein B.R., Russell C.T., and Schubert G.
(1972) Orbital mapping of the lunar magnetic field. Institute of
Geophysics and Planetary Physics, UCLA Publication No. 1092-13.

Sonett C.P., Colburn D.S., Currie R.G., and Mihalov J.D. (1967) The geomagnetic
tail; topology, reconnection, and interaction with the moon. In Physics of
the magnetosphere (editors R.L. Carovillano, J.F. McClay, and H.R. Radoski).
D. Reidel.

Sonett C.P., Schubert G., Smith B.F., Schwartz K., and Colburn D.S. (1971)
Lunar electrical conductivity from Apollo 12 magnetometer measurements:
Compositional and thermal inferences. "Proc. Second Lunar Sci. Conf.
Geochim. Cosmochim. Acta" Suppl. 2, Vol. 3, pp. 2415-2431. MIT Press.

Strangway D.W., Gose W.A., Pearce G.W., and Carnes J.G. (1973) Magnetism and the history of the moon. Proc. of the 18th Annual Conf. on Magnetism and Magnetic Materials, J. Applied Phys. (in press).

Toksöz M.N., Press F., Dainty A., Anderson K., Latham G., Ewing M., Dorman J., Lammlein D., Sutton G., and Duennebier F. (1972) Structure, composition, and properties of lunar crust. "Proc. Third Lunar Sci. Conf. Geochim. Cosmochim. Acta" Suppl. 3, Vol. 3, pp. 2527-2544. MIT Press.

Urey H.C. (1962) The origin of the moon. In The Moon (editors Z. Kopal and Z. K. Mikhailov), pp. 133-148. Academic Press.

Urey H.C. and MacDonald G.J.F. (1971) Origin and histroy of the moon. In Physics and Astronomy of the moon (editor Z. Kopal), pp. 213-289. Academic Press.

Wänkee H., Baddenhausen H., Dreibus G., Quijano-Rico, M., Palme and Teschki F. (1973) Multielement analysis of Apollo 16 samples and about the composition of the whole moon. In "Lunar Science IV" (editors J.W. Chamberlain and C. Watkins) pp. 761-763, Lunar Science Institute, Houston.

Weeks R.A. (1972) Magnetic phases in lunar material and their electron magnetic resonance spectra: Apollo 14. "Proc. Third Lunar Sci. Conf. Geochim. Cosmochim. Acta" Suppl. 3, Vol. 3, pp. 2503-2517. MIT Press.

Zussman J. (1972) The minerology, petrology and geochemistry of lunar samples - a review. The Moon 5, 422-435.

APPENDIX

Consider a radially inhomogeneous two-layer permeable sphere in an initially uniform magnetic field $\underline{H}_o$. In the absence of currents $\underline{H} = -\underline{\nabla}\Phi$ and since $\underline{B} = \mu\underline{H}$, at any point $\underline{\nabla}\cdot\underline{H} = 0$. Therefore Φ satisfies Laplace's equation consistent with the continuity of the normal components of $\underline{B}$ and tangential components of $\underline{H}$ at the spherical boundaries. In the various regions the potentials must be

$$
\Phi = \begin{cases}
-H_o r \cos\theta + \displaystyle\sum_{l=0}^{\infty} \frac{\alpha_l}{r^{l+1}} P_l(\cos\theta) & r > R_1 \\[3mm]
\displaystyle\sum_{l=0}^{\infty} \left(\beta_l r^l + \gamma_l \frac{1}{r^{l+1}}\right) P_l(\cos\theta) & R_2 < r < R_1 \\[3mm]
\displaystyle\sum_{l=0}^{\infty} \delta_l r^l P_l(\cos\theta) & r < R_2
\end{cases}
$$

with R_1 and μ_1 the outer radius and permeability, and R_2 and μ_2 the inner radius and permeability. Using Jackson's (1962) notation conventions we match the boundary conditions

$$
\frac{\partial\Phi}{\partial\theta}(R_1^+) = \frac{\partial\Phi}{\partial\theta}(R_1^-) \qquad \frac{\partial\Phi}{\partial\theta}(R_2^+) = \frac{\partial\Phi}{\partial\theta}(R_2^-)
$$

$$
\frac{\partial\Phi}{\partial r}(R_1^+) = \mu_1 \frac{\partial\Phi}{\partial r}(R_1^-) \qquad \mu_1 \frac{\partial\Phi}{\partial r}(R_2^+) = \mu_2 \frac{\partial\Phi}{\partial r}(R_2^-)
$$

All but the $l = 1$ coefficients vanish leaving the four simultaneous equations

$$
\alpha - R_1^3\beta - \gamma = R_1^3 H_o
$$

$$
2\alpha + \mu_1 R_1^3\beta - 2\mu_1\gamma = -R_1^3 H_o
$$

$$
R_2^3\beta + \gamma - R_2^3\delta = 0
$$

$$
\mu_1 R_2^3\beta - 2\mu_1\gamma - \mu_2 R_2^3\delta = 0
$$

We are interested in α, the induced dipole moment, which is given by

$$F \equiv \frac{\alpha}{H_o R_1^3} = \frac{(2\eta+1)(\mu_1-1) - \lambda^3(\eta-1)(2\mu_1+1)}{(2\eta+1)(\mu_1+2) - 2\lambda^3(\eta-1)(\mu_1-1)}$$

where $\eta = \mu_1/\mu_2$ and $\lambda = R_2/R_1$. The resulting dipolar field in an $(\hat{r}, \hat{\theta}, \hat{\phi})$ spherical coordinate system is

$$\underline{B}_o = \frac{\alpha}{R_1^3}(2\cos\theta\,\hat{r} + \sin\theta\,\hat{\theta}) .$$

We rotate the coordinate system about the $\hat{r}$ (or ALSEP $\hat{x}$) axis so that $\hat{\theta}$ and $\hat{\phi}$ correspond to the ALSEP $\hat{y}$ and $\hat{z}$ axes; then

$$\underline{B}_o = F(2H_x\,\hat{x} - H_y\,\hat{y} - H_z\,\hat{z})$$

The total field at the surface is the sum of the uniform external field $\underline{H}$ and the dipole field $\underline{B}_o$:

$$\underline{B} = H_x(1+2F)\,\hat{x} - H_y(1-F)\,\hat{y} + H_z(1-F)\,\hat{z} .$$

Fig. 1. Induced magnetization of the moon. When a two-layer permeable sphere is immersed in a uniform external magnetic field $\underline{H}$ (in our case the moon in the steady geomagnetic tail field), a dipolar magnetization field $\underline{M}$ is induced with its dipole moment aligned along the direction of $\underline{H}$; the total field near the sphere is $\underline{B} = \underline{H} + 4\pi\underline{M}$. In the case illustrated here, $\mu_1 > \mu_2 > \mu_0 = 1$ (free space), corresponding qualitatively to the case where the outer shell (of radius R_1) contains both ferromagnetic and paramagnetic material, whereas the core (of radius R_2 and temperature above the Curie point) contains only paramagnetic material. Measurements of $\underline{B}$ and $\underline{H}$ allow construction of a classical B-H hysteresis curve for the sphere, from which permeability and iron abundance can be calculated.

Fig. 2. Magnetic environment of the moon during a complete lunar orbit, with emphasis on the geomagnetic tail region. The plane of the lunar orbit very nearly coincides with the ecliptic plane of the earth's orbit. The earth's permanent dipole field is swept back into a cylindrical region known as the geomagnetic tail; at the lunar distance the field magnitude is ~ 10 gammas or 10^{-4} oersteds. Substructure of the tail consists of two "lobes"; the upper or northward lobe has its magnetic field pointing roughly toward the earth, whereas the lower lobe field points away from the earth. The moon is immersed about four days of each orbit in the tail; the moon can pass through either or both lobes (accented portion of orbit), depending upon the characteristics of the particular orbit.

Fig. 3. Simultaneous Apollo 12 and Ames Explorer 35 magnetometer data from a quiet region of the geomagnetic tail, 1970. Vertical scales for the two magnetometers differ due to the existance of a 38 ± 3 gamma remanent magnetic

field at the Apollo 12 surface site. Components of the fields are expressed in the ALSEP coordinate system, which has its origin located on the moon's surface at the Apollo 12 site; the x-axis is directed radially outward from the lunar surface, whereas y and z axes are tangential to the surface, directed eastward and northward, respectively.

Fig. 4. Hysteresis curves for the moon. For each data point the moon is immersed in the external magnetizing geomagnetic tail field $\underline{H}$ (measured by Explorer 35) which is steady over 30-minute or one-hour time intervals; the total magnetic induction is $\underline{B} = \mu\underline{H}$, measured by an Apollo surface magnetometer. Here only the radial (x) components are plotted. In this low-applied-field regime (~ 10 gamma or 10^{-4} Oe), the hysteresis curves are linear and are fitted by least-squares straight lines. (a) Simultaneous Apollo 12 and Explorer data; each data point represents a 30-minute average during quiet times in the geomagnetic tail for four lunations, 1969-1970. (b) Simultaneous 1-hour averages of Apollo 15 and Explorer data for two lunations, 1971.

Fig. 5. The function F versus susceptibility k_1 of the lunar outer shell (refer to equations (2) and (3)). This figure is for the case where the iron Curie temperature isotherm is at core radius $\lambda = R_2/R_1 = 0.85$, as inferred from temperature models illustrated in Fig. 6. Superimposed on the vertical scale are the best value and limits of F calculated from lunar hysteresis curve slopes; the calculated range of F determines possible ranges for susceptibilities of core and shell for this model.

Fig. 6. Temperature profiles for the lunar interior published by various authors: 1. McConnell et al. (1967), 2. Fricker et al. (1967), 3. Hanks and Anderson (1972), 4. Dyal and Parkin (1973), and 5. Sonett et al. (1971). Superimposed is the pressure-dependent Curie temperature for iron (Bozorth, 1951) versus depth in the moon. The Curie point is reached at a position $R/R_{moon} \sim 0.85$ for the "warm" model and ~ 0.7 for a "cold" model.

Fig. 7. Magnetic susceptibility versus density for two minerals at 1600 ^{o}K, olivine $(xFe_2SiO_4 \cdot (1-x)Mg_2SiO_4)$ and orthopyroxene $(xFeSiO_3 \cdot (1-x)MgSiO_3)$, used to model the lunar interior. For a homogeneous moon composed of either of these minerals, the iron silicate concentrations with densities greater than $\rho = 3.34$ gm/cm^3 are forbidden.

Fig. 8. Iron abundance in the moon. Total iron abundance of the moon is calculated for two compositional models of the lunar interior, each with two different thermal profiles. Total iron includes both free iron and iron combined in the paramagnetic state. The portion of the total iron which contributes most strongly to the measured permeability, ferromagnetic free iron, is listed separately.
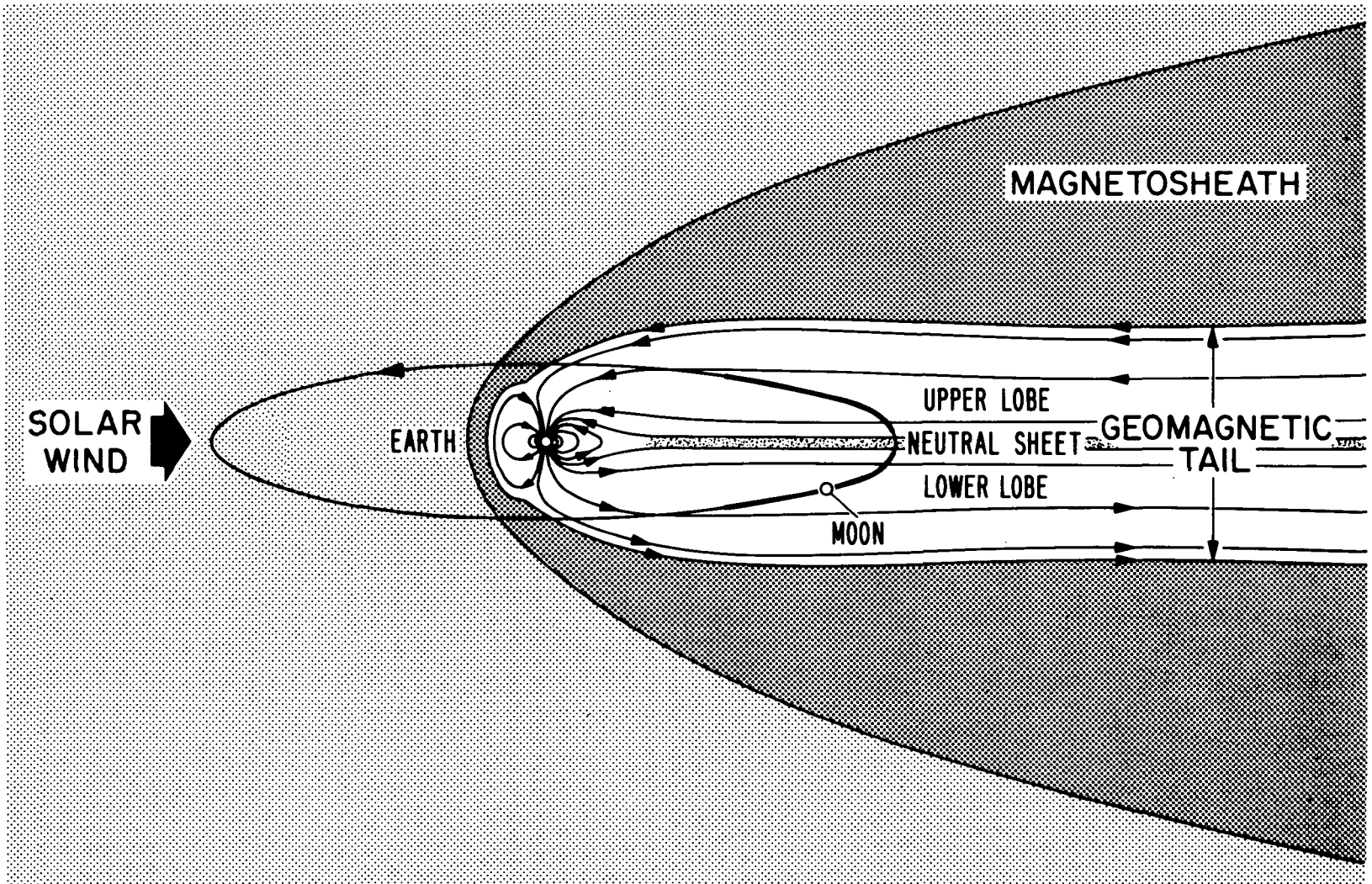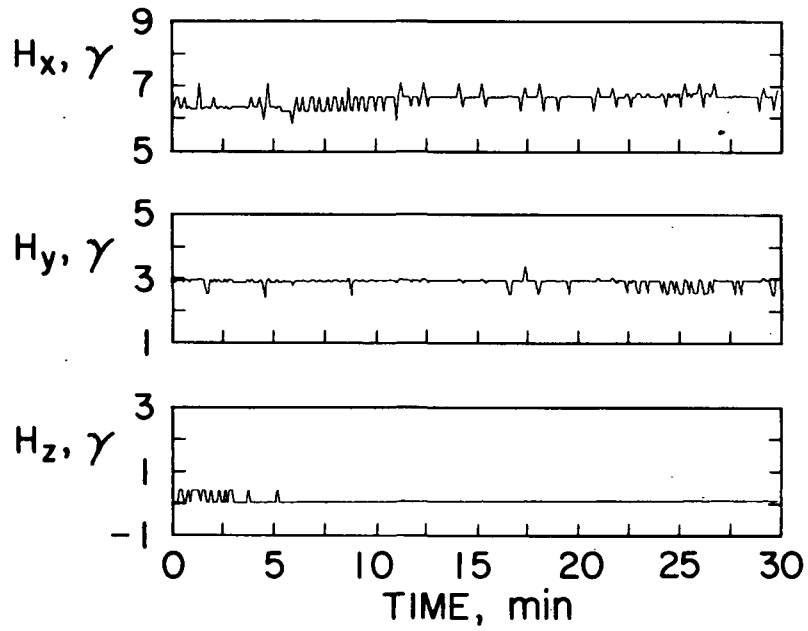
EARTH'S FIELD, $\vec{H}$ FIELD AT MOON, $\vec{B}$

$\vec{H}$

$\vec{B}$

μ_1 μ_2 $\mu_0 = 1$
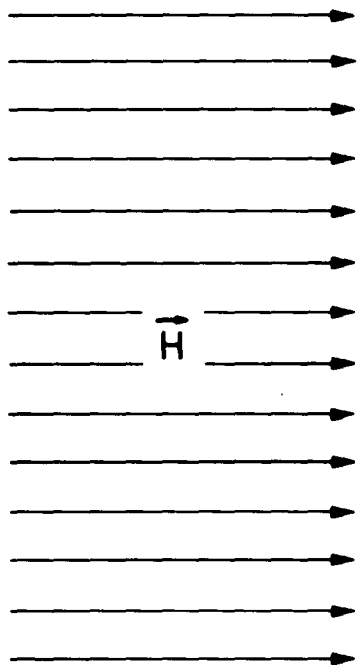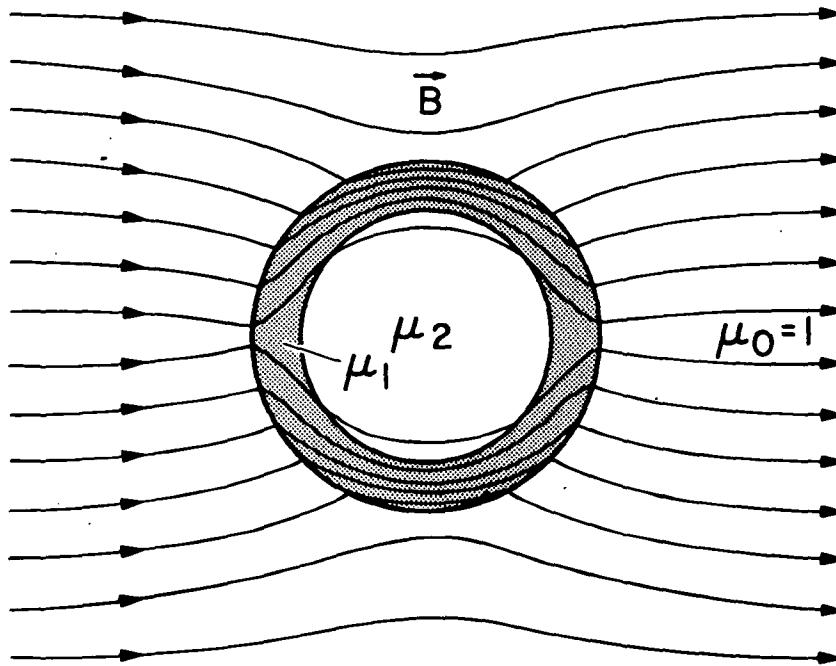
Fig. 1

Fig. 2

MAGNETIC FIELD

EXPLORER 35   APOLLO 12 LSM
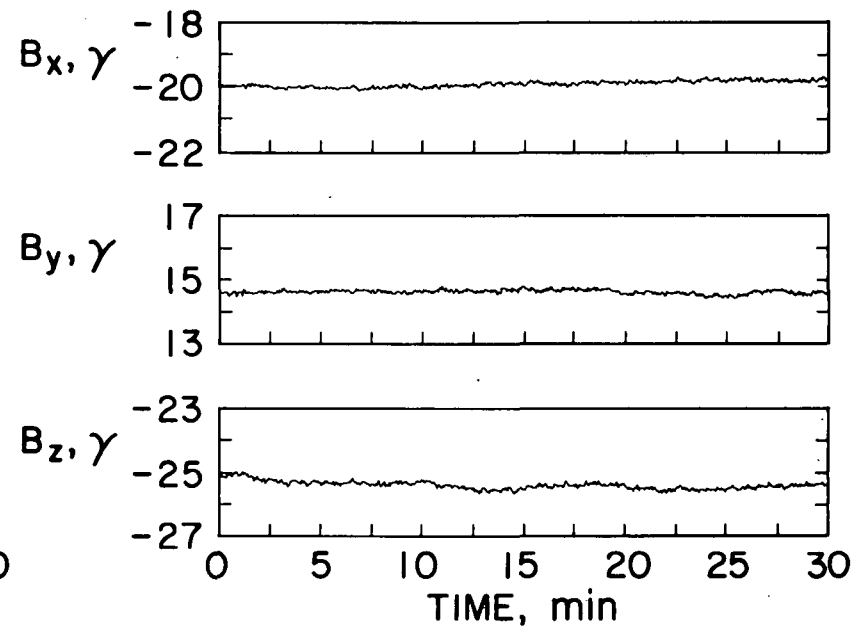
Fig. 3

LUNAR HYSTERESIS CURVES

APOLLO-12 LSM AND EXPLORER-35

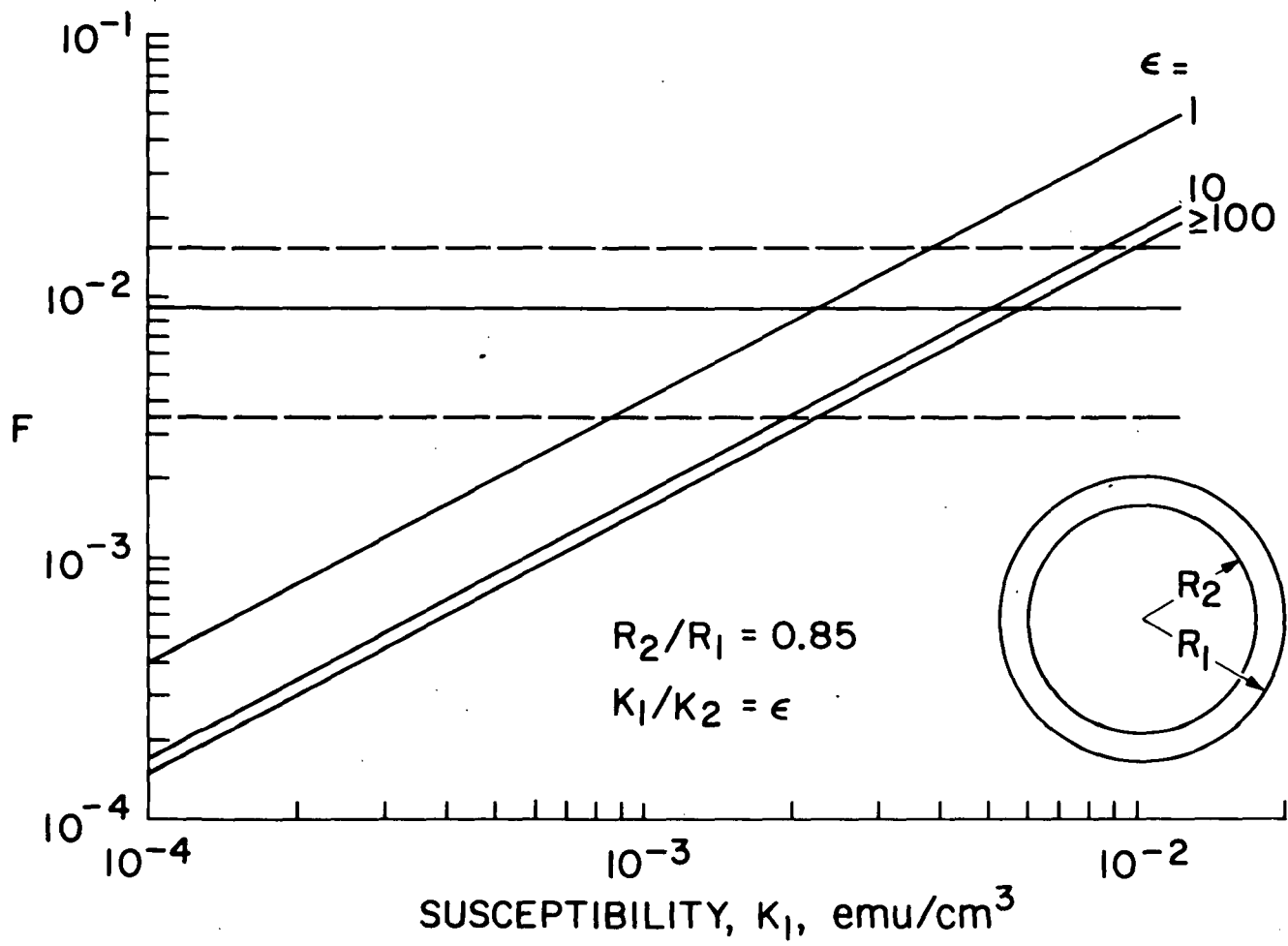APOLLO-15 LSM AND EXPLORER-35
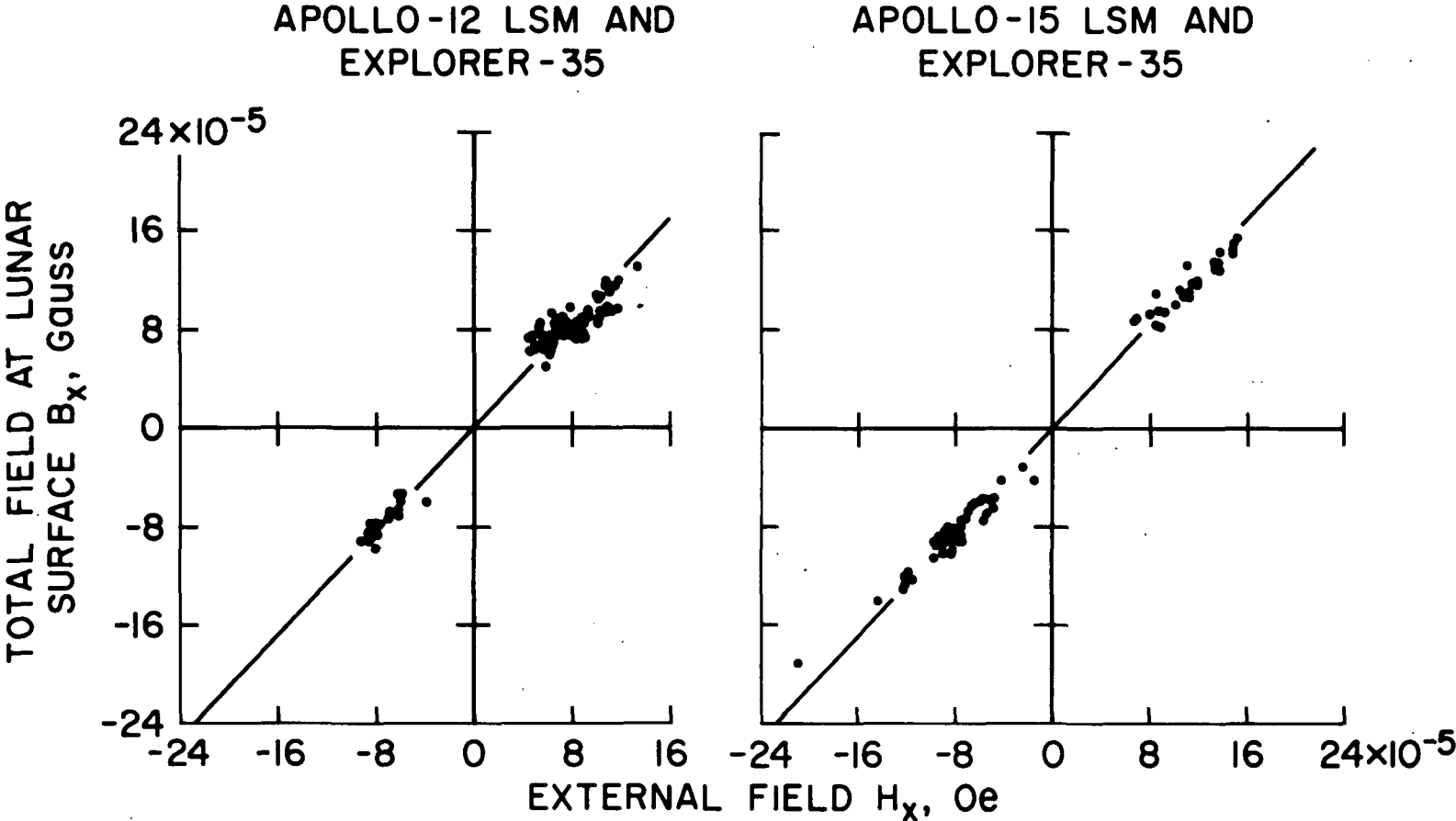
Fig. 4

Fig. 5
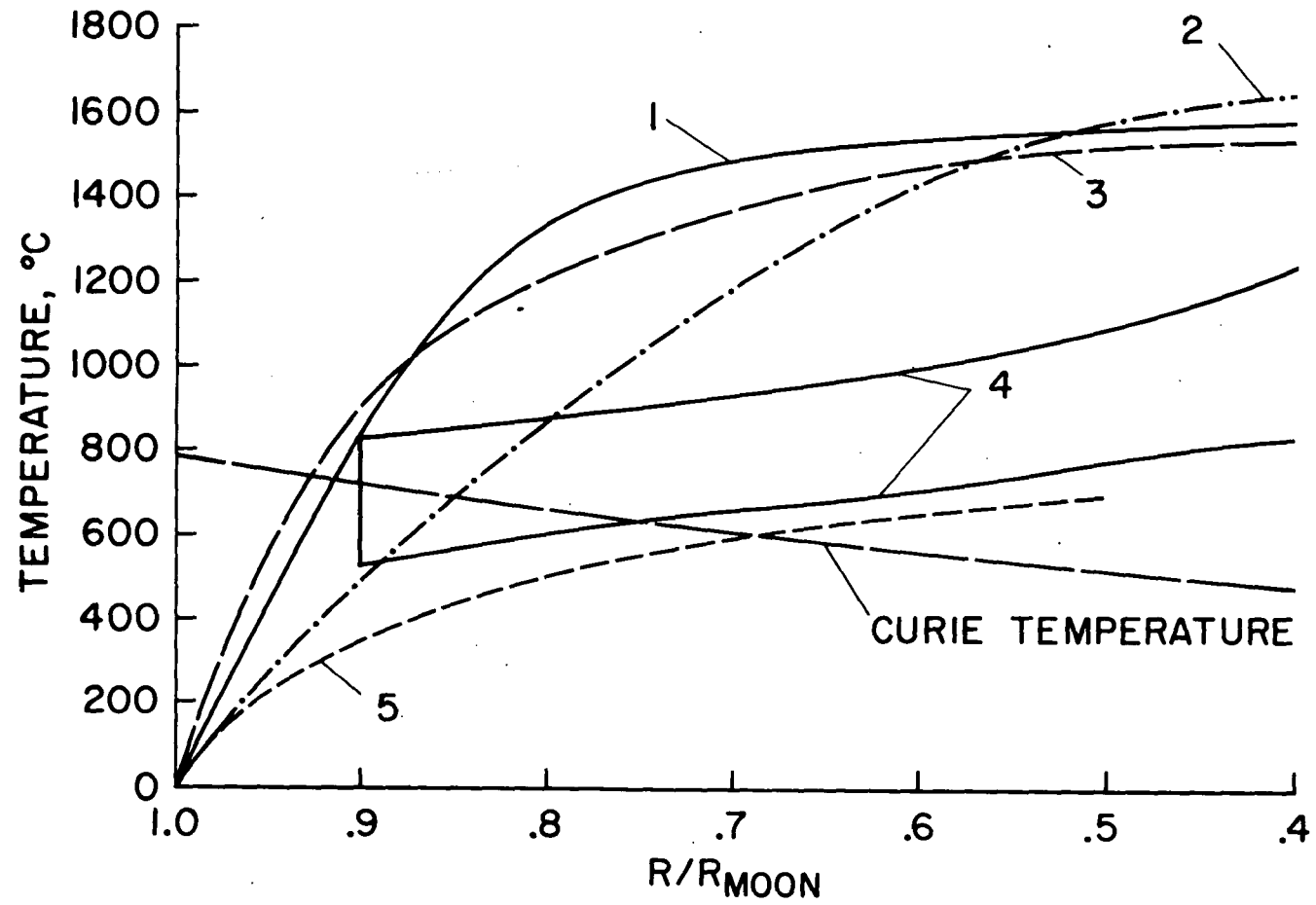
Fig. 6
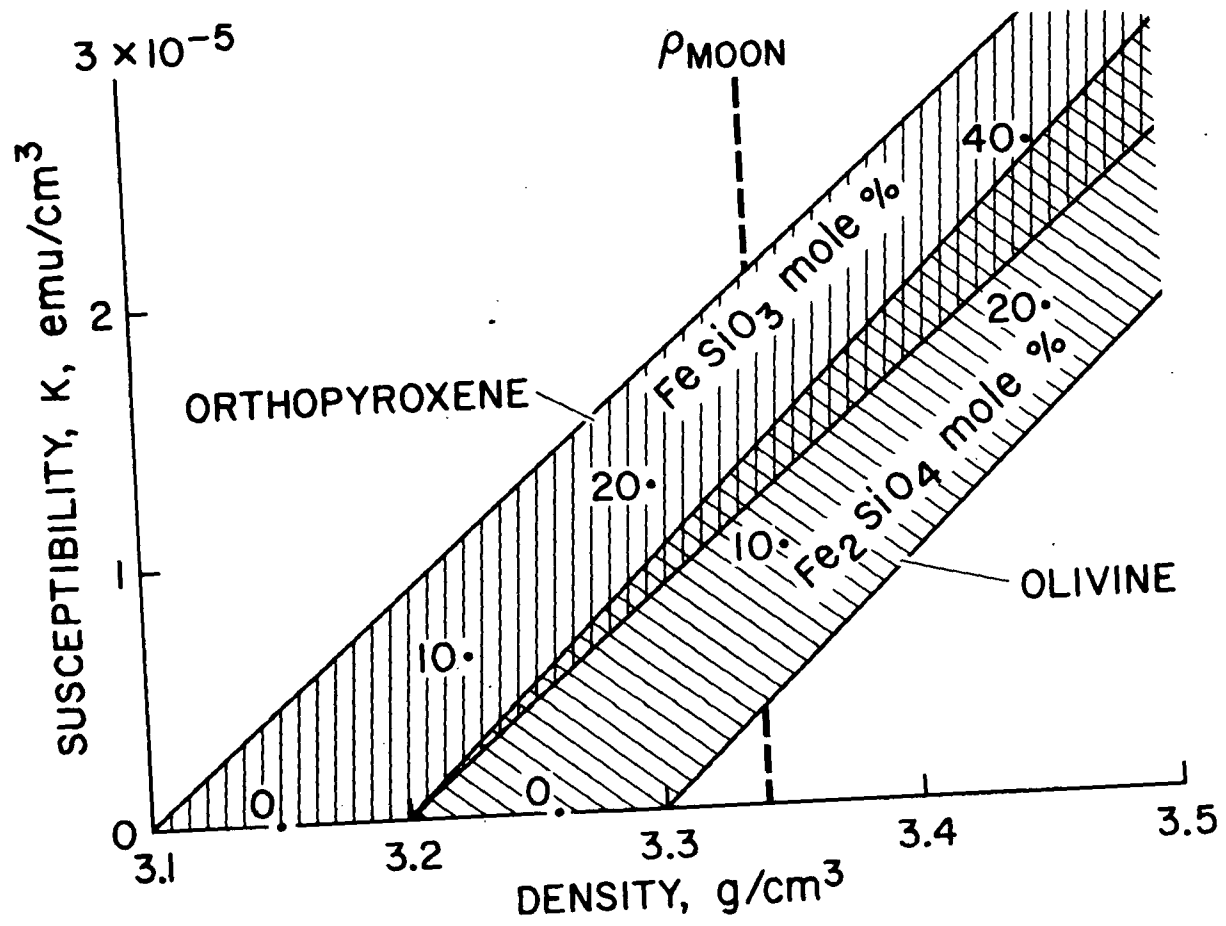
Fig. 7
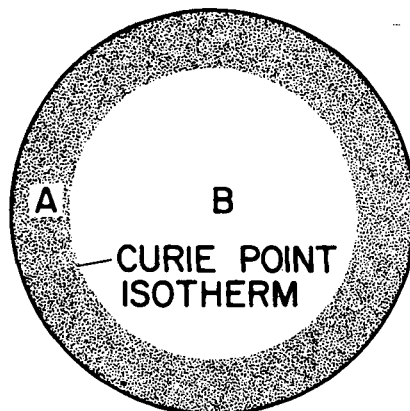
COMPOSITIONAL MODEL	IRON CURIE POINT AT R/R_{moon}	WT % FREE IRON IN SHELL A	TOTAL WT % IRON IN MOON
OLIVINE AND FREE IRON	0.85	2-9	5-6
	0.7	1-5	
ORTHOPYROXENE AND FREE IRON	0.85	2-9	12-13
	0.7	1-5	

Fig. 8